~~Multiphase Reactions~~Liquid-phase reactions of aromatic organosulfates with OH radicals: Kinetics, mechanisms, and environmental effects

Yu Yang[1], Caiqing Yan[1], Ruyu Yuan[1], Ping Liu[1], Hanyuan Zhang[1], Haibiao Chen[1], Yujiao Zhu[1], Hengqing Shen[1], Yan Wu[2], Likun Xue[1] and Liubin Huang[1*]

[1]Environment Research Institute, Shandong University, Qingdao, Shandong 266237, China
[2]School of Environmental Science and Engineering, Shandong University, Qingdao, Shandong 266237, China

Correspondence to: Liubin Huang (hliubin@sdu.edu.cn)

Abstract. Aromatic organosulfates (aromatic OSs) are widely detected in the atmosphere and exhibit high abundance in urban areas. However, the atmospheric fate and environmental impacts of aromatic OSs remain poorly understood. In this study, we investigated the ~~multiphase reaction~~liquid-phase reactions of three aromatic OSs (i.e., phenyl sulfate, p-tolyl sulfate, and 4-ethylphenyl sulfate) with OH radicals (•OH). The second-order reaction rate constants (k) of aromatic OSs with •OH were measured in the range of 4.3–6.4×10^9 M^{-1} s^{-1} at different pHs. It is found that k values are similar for the homologues of aromatic OSs, whereas they are slightly affected by the solution pH values. ~~The multiphase reactions of~~ These three aromatic OSs ~~and~~ oxidized by •OH mainly yielded functionalized OSs, along with fragmented OSs and inorganic sulfate. The observation of inorganic sulfate formation, for the first time, indicates that aromatic OSs can also be converted into inorganic sulfate in analogous to aliphatic OSs. Furthermore, generated ~~chromophores and fluorophores (constituents of brown carbon, BrC) products~~functionalized OSs can significantly enhance the light absorption capacity, particularly under acidic conditions. These findings provide new insights into the understanding of the fate of aromatic OSs in the atmosphere that they can rapidly undergo atmospheric transformation, affecting the atmospheric sulfur cycle and altering aerosol optical properties.

1 Introduction

Secondary organic aerosols (SOA) play a significant role in regional air quality, climate change, and public health (Peng et al., 2023; Shrivastava et al., 2017; Liu et al., 2022). Organosulfates (OSs), organic compounds characterized by a sulfate ester functional group (R–O–SO_3^-), have been widely detected in SOA in various environments (from remote to highly polluted) (Kristensen et al., 2011; Zhang et al., 2012; Hansen et al., 2014; Hu et al., 2015; Wang et al., 2018; Ma et al., 2025), accounting for ~~~~up to 30% of particulate organic mass (Surratt et al., 2008; Lukács et al., 2009; Tolocka and Turpin, 2012; Li et al., 2025). OSs can be produced from the reactions involving biogenic volatile organic compounds (VOCs) such as isoprene and monoterpenes, or anthropogenic VOCs such as diesel fuel vapor and aromatics (Hettiyadura et al., 2019; He et al., 2022; Wang et al., 2022; Thomas et al., 2025). In remote or clean areas, OSs were typically measured with the structure characterization of

isoprene, monoterpenes, and their derivatives (Surratt et al., 2008; Zhang et al., 2012; Hettiyadura~~,~~ et al., 2017). For example, Thomas et al. (2025) reported that IEPOX-OS ($C_5H_{12}O_7S$) is the dominant species of OSs in aerosols in Amazonian rainforest. In urban areas, in addition to isoprene and monoterpenes derived OSs, other OSs containing an aromatic ring ~~(~~were also observed in collected aerosols (Kundu et al., 2013; Huang et al., 2018; Wang et al., 2021; He et al., 2022). He et al. (2022) identified four kinds of aromatic OSs (i.e~~.g~~., phenyl sulfate, methylphenyl sulfate, benzyl sulfate~~) were also ubiquitous in collected aerosols except for isoprene and monoterpenes derived OSs. Kundu et al. (2013) quantified the concentration of benzyl sulfate in the range of~~ and phenethyl sulfate) with concentrations ranging from 0.~~05 to~~04 ± 0.~~508 to 2.37 ± 3.59 ng m^{-3} in $PM_{2.5}$ collected in ~~Lahore, Pakistan, and also identified three additional methyl substituted aromatic OSs (with $C_7H_7SO_4^-$ m/z 187, $C_8H_9SO_4^-$ m/z 201, and $C_9H_{11}SO_4^-$ m/z 215). Ma et al. (2014) reported~~Chengdu, China. Previous study observed that aromatic OSs ~~accounted~~can account for up to 63.5% of the total identified OSs in ~~Shanghai, China. These compounds seem to become more significant when anthropogenic VOCs appear to be the dominant source of SOA.~~a megacity in China (Ma et al., 2014).

Extensive research has been conducted to elucidate the mechanisms of OSs in the atmosphere. The proposed formation mechanisms include: (a) the reactive uptake of epoxides on acidic sulfate aerosols. This pathway was established to be an important mechanism for the formation of isoprene-derived OSs (Surratt et al., 2010; Lin et al., 2013; Riva et al., 2019; Lei et al., 2022); (b) the multiphase reactions of unsaturated hydrocarbons with either sulfate radical ($\bullet SO_4^-$) or sulfur dioxide (SO_2). Previous studies revealed that the addition of $\bullet SO_4^-$ on the C=C bond can result in the formation of OSs in aqueous aerosols (Nozière et al., 2010; Schindelka et al., 2013), and SO_2 can effectively react with unsaturated fatty acids~~, emitted mainly from cooking activities, can directly react with SO_2~~ to form OSs (Shang et al. 2016; Passananti et al. 2016); (c) heterogeneous reaction of organic peroxides with SO_2. Recent laboratory studies have shown that SO_2 can also be oxidized by organic peroxides rapidly with the production of OSs other than sulfate (Wang et al., 2019; Yao et al., 2019, 2023); (d) substitution reaction of organic nitrates (ONs) by sulfate (Darer et al., 2011; Hu et al., 2011). Darer et al. (2011) and Hu et al. (2011) observed the formation of OSs during the processes of ON hydrolysis in the presence of H_2SO_4; (e) acid-catalyzed esterification of alcohols. While laboratory studies reported OS formation from sulfate esterification (Iinuma et al., 2007), subsequent kinetic study suggested that this reaction is too slow under typical tropospheric conditions (Minerath et al., 2008).

Compared to the formation of OSs, understanding of the fate of OSs is still limited. Hydrolysis has been identified as ~~a potential~~an atmospheric removal process for certain OSs, with rates depending on the acidity of the aerosol and the molecular structure (Darer et al., 2011; Hu et al., 2011; Mael et al., 2015). Tertiary OSs were found to hydrolyze effectively under acidic conditions, while primary and secondary OSs were relevantly stable. Additionally, OSs can also be further ~~undergo the~~oxidized by OH radicals (•OH) after formation. Lai et al. (2024) investigated the kinetics of ~~OH radicals reacted with~~ reactions of methyl sulfate and ethyl sulfate with •OH, finding that the rate constant (k) may be significantly affected by the carbon chain length. ~~k value of ethyl sulfate ($3.8 \pm 0.1 \times 10^8$ L mol^{-1} s^{-1}) was approximately five times higher than that of methyl sulfate ($7.5 \pm 0.1 \times 10^7$ L mol^{-1} s^{-1}). This observation~~This finding was also verified in ~~the border~~more kind of aliphatic OSs (i.e., methyl sulfate, ethyl sulfate, and propyl sulfate)~~ with the possible explanation of the inductive effects of the additional CH_x groups, which can~~

~~enhance electron density at the H-abstraction site and stabilize the formed alkyl radical~~ (Gweme and Styler, 2024). Chen et al. (2020a) detected the products of 2-methyltetrol sulfate diastereomers (IEPOX-OS) oxidized by •OH heterogeneously, observing varied fragmented and functionalized OSs after reactions, which their formation pathways were previously unknown in the atmosphere. ~~Except for new OSs formed, previous study also pointed out that partial of OSs can return back to inorganic sulfate during~~During the ~~reaction~~oxidation of ~~OH radicals with~~some OSs (e.g., methyl sulfate, ethyl sulfate, 2-methyltetrol sulfate, and α-pinene derived OSs~~), indicating that~~) by •OH, it ~~may significantly contribute to the atmospheric sulfur cycle~~is interesting to find that OSs can also return to inorganic sulfate except for new OS formation (Kwong et al., 2018; Xu et al., 2020~~).~~, 2024). In addition to laboratory studies, Tsona et al. (2025) employed quantum chemical calculation based on density functional theory to confirm the formation of inorganic sulfate from the gas-phase and aqueous-phase reactions of OSs with •OH. It should be noted that the currently limited research about the fate of OSs has focused on the biogenic OSs or small alkyl OSs, little is known about the kinetic and mechanism for the conversion of aromatic OSs, which is another important kind of OSs, particularly in the urban aerosols. A very recent study investigated the aqueous-phase •OH oxidation of phenyl sulfate other than aliphatic OSs (Gweme and Styler, 2024), observing that the *k* value of phenyl sulfate is much faster than that of aliphatic OSs. After reactions, they observed the new OSs formed (hydroxyphenyl sulfate and dihydroxyphenyl sulfate), but without any evidence of inorganic sulfate production. However, whether aromatic OSs can be converted into inorganic sulfate or not remains unclear since they did not observe the presence of inorganic sulfate for aliphatic OSs as well. Therefore, to better characterize and understand the ~~multiphase reaction~~liquid-phase reactions of aromatic OSs and •OH, further research is warranted.

In this study, we investigated the ~~multiphase reaction~~liquid-phase reactions of atmospherically relevant aromatic OSs (i.e., phenyl sulfate, p-tolyl sulfate, and 4-ethylphenyl sulfate) with •OH ~~(He et al., 2022)~~. Our study aims to explore the influence of substituent structure on reaction kinetics and elucidate the mechanisms for the conversion pathways of aromatic OSs in the atmosphere~~, and examine~~. Moreover, given that the ~~change~~oxidation of aromatic organic compounds often induces significant alteration in the optical properties of the reaction system (Li et al., 2021; Arciva et al., 2024), the changes of optical properties were also examined.

2 Materials and methods

2.1 Batch reactor experiments

Experiments of the liquid-phase •OH oxidation of aromatic OSs were carried out in a 150 mL custom-built quartz reactor thermostated by a water jacket. OH radicals were generated through the aqueous photolysis of 10 mM H_2O_2 (30%, Hu Shi) under irradiation from a 300 W Xenon arc lamp to simulate sunlight. Three commercial aromatic OSs (i.e., phenyl sulfate (≥98%, Macklin), p-tolyl sulfate (≥98%, Macklin), and 4-ethylphenyl sulfate (≥98%, Sigma-Aldrich)) were used as the representatives of aromatic OSs. Their structures are shown in Fig. S1. The reaction solution containing each aromatic OS, H_2O_2, and dissolved O_2 was introduced into the quartz reactor with a total volume of 100 mL, and was agitated by an

electromagnetic stirrer. Subsequently, the reactor was sealed, and the lamp was then ignited to start the reaction. Given ~~that~~ the varied pH ~~of atmospheric water-containing particles typically ranges~~ values in aqueous environments in the atmosphere (from 1 to 9) (Herrmann et al., 2015; Pye et al., 2020), the solution was adjusted to pH 3 (using 36–38% HCl, Hu Shi) and pH 8 (using phosphate buffer (Na_2HPO_4 and NaH_2PO_4)) to represent acidic and alkaline conditions, respectively. All experiments were performed at 298 K ~~for 2~12 h of reaction time. The initial concentration of OS was 0.05 mM. Additional experiments with elevated concentrations of OSs (0.5 or 1 mM) were carried out in order to observe obvious product signals and optical change characteristics.~~in at least duplicate. Details about the information of the experiments carried out in this study are summarized in Table S1.

Kinetic experiments were performed with 0.05 mM of each aromatic OS in the presence of reference compound (i.e., sodium benzoate (BA, 98%, Macklin)) in the reaction time of 2 hours. Two sets of control experiments were carried out. One involved irradiating a solution of each aromatic OS alone to investigate the effects of light only. Another set combined each aromatic OS and H_2O_2 in the dark to preclude the interference of H_2O_2. Reaction progress was tracked by withdrawing 1 mL aliquots at 30-minute intervals for direct analysis via either ultrahigh-performance liquid chromatography (UPLC, Agilent 1260) or ion chromatography (IC, Dionex ICS-600), without any intermediate processes or dilution. Mechanism experiments were conducted the same as the kinetic experiments, except that BA was not added. After reactions, 0.5 mL of the sample was taken and was immediately stored at –20 ℃ prior to product analysis using ultra-performance liquid chromatography equipped with quadrupole time-of-flight mass spectrometer (UPLC-Q-TOF-MS, Bruker Impact HD). Control experiments of each aromatic OS and H_2O_2 in the dark were also performed as the comparison in order to eliminate the possibility of detected products resulting from analytical artifacts. To enhance the detection of optical changes, we also conducted experiments at higher aromatic OS concentrations (0.5 or 1 mM) over an extended period of 8 hours. For these experiments, the sample was taken every 4 hours for immediate measurement of their absorbance spectra using UV–vis spectrophotometer (Duetta™, Horiba Scientific) and excitation–emission matrix (EEM) fluorescence spectra by a fluorescence spectrometer (Duetta™, Horiba Scientific). After reactions, the sample was also analyzed by ultrahigh-performance liquid chromatograph coupled with a photodiode array detector and an Orbitrap mass spectrometer (UPLC-PAD-MS, Thermo Fisher Scientific) to investigate how optical changes were affected by the formation of chromophores. 0.5 mL sample was diluted by 0.5 mL H_2O and 0.25 mL acetonitrile, and then the resulting solution was stored at –20 ℃ before analysis.

2.2 Kinetic measurements

The second-order rate constant of each aromatic OS with •OH was measured by the competition kinetic method using 0.05 mM sodium benzoate as the reference compound (Smith et al., 2015). ~~For the kinetic studies, 0.05 mM aromatic OS, BA, and 10 mM H_2O_2 were mixed in a quartz reactor, and the following reactions (R1 and R2) were conducted: Assuming~~It is noted that one of important principles of this method is that aromatic OS and the reference compound are consumed only by •OH oxidation in the aqueous phase. Control experiments of the direct photolysis of each aromatic OS without the addition of H_2O_2 as well as the reactions of each aromatic OS, BA, and 10 mM H_2O_2 without illumination were carried out to preclude the

interference of other reactions. Figures. S2 and S3 show that the influences of either hydrolysis or photodegradation on the kinetic measurements of these three aromatic OSs are negligible, verifying that the decay of reactants resulting from •OH oxidation. Therefore, in this study, the second-order rate constant for aromatic OS (k_{OS}) can be calculated using the equation E1~~:~~ based on the following reactions (R1 and R2).

$$\ln\left(\frac{[OS]_0}{[OS]_t}\right) = \frac{k_{OS}}{k_{ref}} \ln\left(\frac{[ref]_0}{[ref]_t}\right) \quad \text{(E1)}$$

$$\text{Aromatic OS} + \bullet\text{OH} \rightarrow \text{Products}, k_{OS} \quad \text{(R1)}$$

$$\text{Reference} + \bullet\text{OH} \rightarrow \text{Products}, k_{ref} \quad \text{(R2)}$$

Where [OS] and [ref] are concentrations of aromatic OS and the reference compound (BA) (time =0 and t). The time dependence of aromatic OS consumption is shown in Fig. S4. k_{ref} is the rate constant of BA with •OH. k_{ref} values at pH 3 and 8 were reported as $4.3 \pm 0.8 \times 10^9$ M^{-1} s^{-1} and $6.3 \pm 0.2 \times 10^9$ M^{-1} s^{-1}, respectively (Buxton et al., 1988). Figure 1 displays the relative kinetic plots for aromatic OSs oxidized by •OH under acidic (pH 3) and basic (pH 8) conditions. These plots exhibit strong linearity ($R^2 \geq 0.99$), with the slope of each linear fit corresponding to the k_{OS}/k_{ref}. According to the ~~slopes and value of k_{ref}, the k_{OS} of the three aromatic OSs can be calculated. As the comparison, we also measured the rate of ethyl sulfate through this relative kinetic method. k_{OS} of ethyl sulfate was measured as $4.57 \pm 0.67 \times 10^8$ M^{-1} s^{-1} at pH 8 (Fig. S3). This value aligns well with the reported $3.85 \pm 0.24 \times 10^8$ M^{-1} s^{-1} at pH 9 (Gweme and Stylerl, 2024), further indicating the reliability of method employed in this study~~slope and value of k_{ref}, the k_{OS} can be calculated.

~~In order to eliminate the interference of other reactions to the kinetic process, two control experiments were also conducted: (1) a dark control under identical conditions except no illumination, and (2) a direct photolysis control under the same conditions but without the addition of H_2O_2. As shown in Fig. S4 and S5, results of the dark reaction of H_2O_2 and the photolytic degradation experiments both exhibited a negligible influence on the concentrations of aromatic OSs.~~

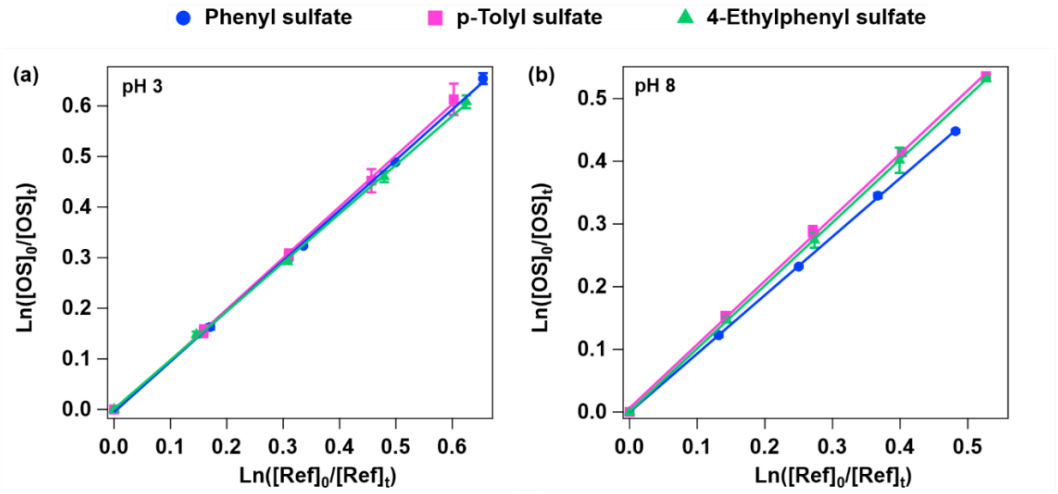

Figure 1. Loss of aromatic OSs and BA during the process of the liquid-phase •OH oxidation at (a) pH 3 and (b) pH 8.

2.3 Reactant and product analysis

The concentrations of aromatic OSs and BA were detected using an ultrahigh-performance liquid chromatography (UPLC, Agilent 1260) coupled with a UV detector operating at 254 nm. Chromatographic separation was performed on a ZORBAX Eclipse Plus C18 column (4.6 mm × 250 mm, 5 μm) maintained at 40 °C. The mobile phase consists of acetonitrile and 0.1% formic acid aqueous solution (20:80, v/v) delivered at a flow rate of 0.8 mL min^{-1}, with an injection volume of 10 μL. Quantification of aromatic OSs and BA was achieved by calibration curves (Fig. S5), based on their corresponding peak areas in the chromatogram.

Inorganic sulfate was analyzed by IC with an analytical column (AS 11-HC, 4 × 250 mm; IonPac) and a guard column (AG11-HC, 4 mm × 250 mm, IonPac). The eluent was 20 mM potassium hydroxide at a flow rate of 1 mL min^{-1}.

~~The products were detected using two liquid chromatography-mass spectrometry (LC-MS) systems: an ultra-high performance liquid chromatography coupled with quadrupole time-of-flight mass spectrometry (Bruker Impact HD, Germany) and an ultra-high performance liquid chromatography (UltiMate 3000) coupled to a Q Exactive oeus Hybrid Quadrupole-Orbitrap mass spectrometry (Thermo Scientific, USA). Details about the methods can be seen in the supporting information (Sections S1and S2). The sample preparation is as follows: Aliquots (0.5 mL) were collected from the reactor at predetermined time intervals. To quench residual H_2O_2, each aliquot was immediately mixed with an equal volume of catalase solution (~0.1 mg mL^{-1}) prepared in phosphate buffer (pH 7) to both neutralize the reaction mixture pH and maintain enzyme activity. The samples were then incubated with catalase at 25 °C for 15 min. Following incubation, 250 μL of acetonitrile was added, and the solution was filtered through a 0.22 μm PTFE syringe filter before analysis. In addition, complementary analyses were carried out by mass spectrometry using the direct infusion mode under the negative ionization mode. Phenol generated in the experiment was verified by ultrahigh-performance liquid chromatography equipped with a fluorescence detector (UPLC-FLD), the method was detailed in Section S3.~~

Reaction products were detected using a UPLC-Q-TOF-MS. Separation was achieved on a C18 column (4.6 mm × 250 mm, particle size = 5 μm; ZORBAX Eclipse Plus) at 40 °C, with a mobile phase of pure water and acetonitrile (40:60, v/v) at a flow rate of 1 mL min^{-1}. The mass spectrometer was equipped with an electrospray ionization (ESI) source operated in the negative (-) ionization mode. The instrumental conditions for the (-) ESI-MS analysis were as follows: capillary voltage, 4000 V; gas temperature, 200 °C; dry gas flow rate, 5 L min^{-1}; and nebulizer pressure, 0.4 bar. Data were collected over the mass range of 50–500 Da. We also conducted complementary chromophore product analyses using a UPLC-PAD-MS. Separation was carried out a C18 column (4.6 mm × 250 mm, particle size = 5 μm; ZORBAX Eclipse Plus) at 40 °C, with a binary mobile phase consisting of acetonitrile and 0.1% formic acid (20:80, v/v) delivered at a flow rate of 0.8 mL min^{-1}. Mass spectrometric detection was conducted in negative ionization mode over a mass range of 50–500 Da, with the spray voltage set at –3.0 kV, the capillary temperature at 320 °C, the S-lens RF level at -50V, the sheath gas (nitrogen) pressure at 2.76×10^5 Pa, and the auxiliary gas (nitrogen) flow rate at 3.33 L min^{-1}.

2.4 UV-vis absorption and fluorescent spectra

The light absorption spectra of samples during the processes of reactions were collected using a UV–vis spectrophotometer with a scanning interval of 1 nm in the range of 250–700 nm. A reference absorption spectrum of hydrochloric acid solution (pH 3) or phosphate buffer solution (pH 8) was recorded in the same cuvette before sample analysis for baseline correction. The excitation-emission matrix (EEM) fluorescence spectra were recorded by a fluorescence spectrometer. The excitation wavelength (Ex) and emission wavelength (Em) of EEM were both set to the range of 250–600 nm. The scanning intervals were set to 5 nm and 2 nm. hydrochloric acid solution (pH 3) or phosphate buffer solution (pH 8) was used as a blank to correct the data as well.

3 Results and discussion

3.1 Kinetics of liquid-phase reaction of aromatic OSs with •OH

The k_{OS} values of three aromatic OSs (i.e., phenyl sulfate, p-tolyl sulfate, and 4-ethylphenyl sulfate) are summarized in Table 1 reacted with •OH. At pH 3, the k_{OS} value of phenyl sulfate was measured as $4.3 \pm 0.1 \times 10^9$ M^{-1} s^{-1}. This value is comparable to the literature result of phenyl sulfate at pH 2 using pimelic acid as the reference compound ($5.34 \pm 0.06 \times 10^9$ M^{-1} s^{-1}) (Gweme and Styler, 2024). The slight difference may be attributed to the reference compound selection and the experimental conditions. Values of k_{OS} for the other two aromatic OSs were similar to that of phenyl sulfate. The similar k_{OS} value among these three aromatic OSs suggests that the substituent carbon chain length on the aromatic ring has a negligible effect on the reaction kinetics. This observation is quite different from that for alkyl OSs, which shows that k_{OS} is strongly dependent on the carbon number of OS molecule contained (Armstrong et al., 2022; Yan et al., 2023; Lai et al., 2024; Gweme and Styler, 2024). Lai et al. (2024) reported that k_{OS} of ethyl sulfate ($3.8 \pm 0.1 \times 10^8$ M^{-1} s^{-1}) was approximately five times higher than that of methyl sulfate ($7.5 \pm 0.1 \times 10^7$ M^{-1} s^{-1}). Gweme and Styler (2024) also found that k_{OS} value increased with increasing carbon

chain length for methyl sulfate~~,~~ (1.03 ± 0.21 × 10^8 M^{-1} s^{-1}), ethyl sulfate~~,~~ (4.07 ± 0.17 × 10^8 M^{-1} s^{-1}), and propyl sulfate~~.~~ (1.22 ± 0.03 × 10^9 M^{-1} s^{-1}). This distinct ~~behavior~~behaviour may be ascribed to the different mechanisms for aromatic OSs and alkyl OSs oxidized by •OH. For aromatic OSs, the OH radical predominantly attacks the aromatic ring with multiple addition sites (Bloss et al., 2005; Garmash et al. 2020). While alkyl OSs react primarily through hydrogen abstraction, the increasing carbon chain length can enhance reactivity through the inductive effect of $-CH_x$ groups, the increasing electron density at the hydrogen abstraction site, and the stabilization of resulting alkyl radicals (Monod and Doussin, 2008; Dorfman and Adams, 1973). As such, aromatic OSs has higher reactivity compared to alkyl OSs. The negligible effect of carbon number on the reactivity of aromatic compounds was also observed in other structure of homologue of aromatics. For example, Schuler and Albarran. (2002) reported a similar rate constant for the reactions of toluene (8.1×10^9 M^{-1} s^{-1}) and benzene (7.8×10^9 M^{-1} s^{-1}) with OH radicals. It is noted that the k_{OS} values are lower than those of their parent aromatic hydrocarbons. This reduction in reactivity may be attributed to the electron-withdrawing effect of the $-OSO_3^-$ groups, which can reduce the reactivity of the aromatic ring toward •OH (Lai et al., 2024).

Table 1. The second-order rate constant (*k*) of aromatic OSs reacting with •OH in the liquid phase at different pHs.

Species	*k* (10^9 M^{-1} s^{-1})	
	pH = 3	pH = 8
Phenyl sulfate	4.3 ± 0.1	5.9 ± 0.1
p-Tolyl sulfate	4.4 ± 0.1	6.4 ± 0.2
4-Ethylphenyl sulfate	4.5 ± 0.1	6.3 ± 0.1
Benzoic acid[a]	4.3 ± 0.8	6.3 ± 0.2

[a] Rate constants for benzoic acid are obtained from Buxton et al. (1988).

Table 1 shows that the carbon chain length has an insignificant effect on the k_{OS} values of aromatic OSs at pH 8 as well. k_{OS} values of phenyl sulfate, p-tolyl sulfate, and 4-ethylphenyl sulfate were calculated as 5.9 ± 0.1 × 10^9, 6.4 ± 0.2 × 10^9, and 6.3 ± 0.1 × 10^9 M^{-1} s^{-1}. These values were higher than those measured at pH 3. It should be noted that different matrices (HCl *vs* phosphate buffer) were used to adjust the solution pH, and the ionic strength of the solution is different at different pHs. The ionic strengths of solution at pH 3 and pH 8 were estimated as 1 × 10^{-3} M and 6.9 × 10^{-3} M, respectively. Previous study reported that a substantial increase in ionic strength from ca. zero to 6.5 M only resulted in a tenfold decrease in k_{OS} value of phenyl sulfate (Gweme and Styler, 2024). Therefore, the relatively low ionic strength variation between pH conditions in this study may not account for the observed differences in the k_{OS} values of aromatic OSs. Gweme and Styler (2024) measured the k_{OS} of phenyl sulfate at pH 2 and pH 9, observing that it was pH independence. They attributed this pH independence to phenyl sulfate remaining fully deprotonated (pKa = –2.2) across the entire experimental pH range. However, previous studies demonstrated that even though methoxyphenol, benzene-diols, and highly substituted phenol mainly exist in their protonated form within the pH range of 2–6, their *k* values at pH 2 was generally lower than those at pH 5 or 6 (Arciva et al., 2022). ~~This phenomenon may arise from several factors: (1)~~On possible explanation is that the acidic condition could hinder •OH attack on aromatic systems or reduce the lifetime of hydroxyl-cyclohexadienyl radical intermediates, slowing irreversible diol

formation (Smith et al., 2015). ~~(2) The~~ Another possible explanation is the uncertainty of the k of the reaction of reference compound with •OH (Arciva et al., 2022). Therefore, the difference and uncertainty of the rate constant of the reference compounds selected may also ~~be the reason for~~explain the discrepancy between that reported by Gweme and Styler (2024) and our study~~. Moreover, pronounced variations in product distributions under differing pH conditions imply the involvement of distinct reaction pathways. The mechanistic divergence likely serves as a key factor for the observed pH dependence of k_{OS} values~~.

3.2 Product measurements and reaction mechanism

~~Products~~In this study, products generated from the liquid-phase reactions of three aromatic OSs ~~after reaction~~ with •OH were ~~also detected~~characterized by ~~the~~ mass spectrometry. The identified species were consistent across both under pH 3 and pH 8 conditions. The observation that product intensities were substantially higher under illumination conditions than in dark controls implies that these products arise from •OH oxidation, not from analytical artifacts or hydrolysis (Fig. S6).~~spectrometer.~~ Table S2 lists the identified products from the reaction of phenyl sulfate with •OH. The predominant signals corresponded to hydroxyphenyl sulfate ($C_6H_5O_5S^-$, *m/z* 189) and dihydroxyphenyl sulfate ($C_6H_5O_6S^-$, *m/z* 205), aligning with previous work (Gweme and Styler, 2024). Additionally, the multiple –OH group addition products (e.g., $C_6H_5O_7S^-$, $C_6H_7O_8S^-$, and $C_6H_7O_9S^-$, were also detected. As illustrated in Fig. 2, •OH-initiated oxidation of phenyl sulfate follows a mechanism analogous to conventional aromatic compounds~~.~~ (e.g., benzene). The reaction initiates via the addition of •OH to the aromatic ring, generating hydroxycyclohexadienyl radicals (OH-PS radicals) (Lay et al., 1966; Minakata et al., 2015). OH-PS radicals rapidly react with O_2 to yield phenolic compounds that can undergo further multi-step •OH additions to form these polyhydroxy products ($C_6H_5O_nS^-$, n=5–8). Alternatively, OH-PS radicals can also react with O_2 to form peroxyl radicals (RO_2•). The reversible cyclization of RO_2• and the subsequent O_2 addition generate bicyclic RO_2•. Bicyclic RO_2• can react with RO_2• to produce ring-opening products as shown in Table S2 (Wang et al. 2013; Dong et al. 2021). Fragmented OS formation resulting from ring-opening pathways during •OH oxidation of aromatic OSs has not reported previously~~, and partial~~. Notably, some of ~~them~~these ring-opening fragments (e.g., $C_2H_3O_5S^-$~~; $C_3H_5O_4S^-$, $C_3H_7O_5S^-$, $C_5H_5O_6S$~~, $C_5H_7O_8S^-$) have the same formula of OSs detected in the atmosphere, which their precursors were ~~still remain unidentified~~ (regarded as biogenic VOCs (Kuang et al., 2016; Cai et al., 2020; ~~Huang et al., 2023) or are regarded as biogenic VOCs (Cai et al., 2020; Kuang et al., 2016;~~ Wang et al., 2022). For example, previous studies inferred that *m/z* 139 ($C_2H_3O_5S^-$) ~~observed in this study was heretofore considered to be~~is produced from isoprene and its derivates related reactions (Cai et al., 2020; Wang et al., 2022). In this study, we found that this compound can also be formed through the oxidation of phenyl sulfate by •OH, providing the additional pathway for its formation in the atmosphere ~~(Cai et al., , 2020; Wang et al., 2022). These findings suggest that aromatic OSs may serve as a potential source for aliphatic OSs.~~

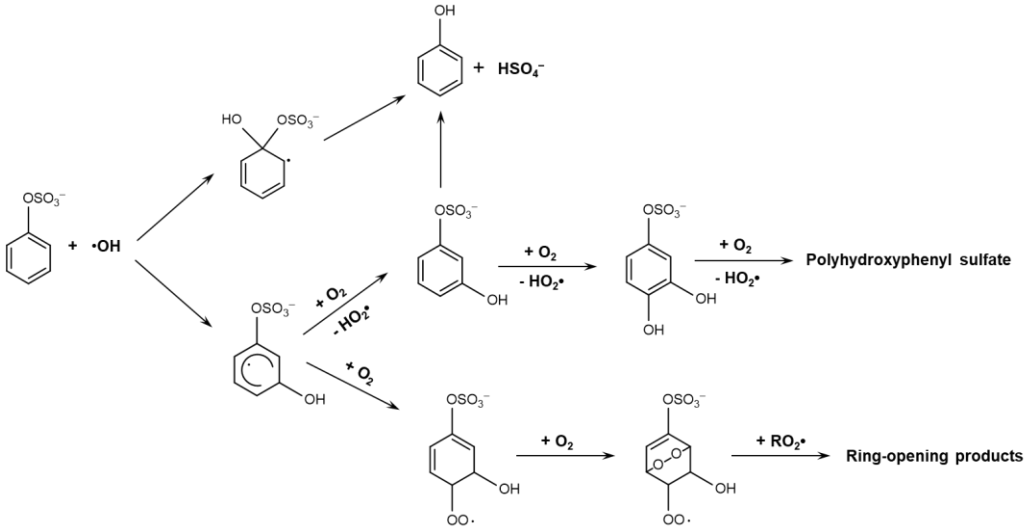

Figure 2. Scheme for the mechanism of phenyl sulfate reacting with •OH.

~~Intriguingly, in addition to the new OSs observed, the formation of inorganic sulfate (HSO_4^-, m/z = 97) was also detected.~~ Previous studies revealed that ~~partial of~~some aliphatic OSs (e.g., methyl sulfate, ethyl sulfate, 2-methyltetrol sulfate, and α-pinene-derived OS) can be converted into inorganic sulfate during •OH oxidation~~. The molar yield of inorganic sulfate was estimated from 46±2% to 62± 18% for the studied OSs ((Kwong et al., 2018; Xu et al., 2022, 2024;~ Lai et al., 2025~~; Xu et al., 2020). The oxidation mechanism of methyl sulfate~~). The reaction is initiated through hydrogen abstraction from the alkyl group~~ by OH radicals~~, forming an alkyl radical~~. The alkyl radical reacts~~ (R•) followed by rapidly reacting with O_2 to form ~~the~~ RO_2 ~~radical. RO radicals, generating from the~~ •. The self- or cross-reactions of RO_2• can further ~~reaction of RO_2~~produce an alkoxy radical~~, can undergo β-scission to generate formaldehyde and~~ (RO•). Typically, the formation of inorganic sulfate ~~anions (•~~is resulted from the production of •SO_4^-~~), thereby producing HSO_4^-. In this~~ , which is generated from the decomposition of α-OSO_3^- alkoxy radical (defined as the containing of -OSO_3^- group at the α-position of RO•). Additionally, a recent study~~, the observation of a pronounced signal of (HSO_4^-, m/z = 97) suggests that aromatic OSs can also return to inorganic sulfate, similar to aliphatic OSs. The result of the control experiment verifies that the pathway of phenyl sulfate hydrolysis can be excluded since the concentration of phenyl sulfate did not change within 2 h of reaction under the same conditions without UV (Fig. S4). It is noted that we also observed~~ proposed an alternative mechanism for the formation of ~~phenol in addition to the observation~~inorganic sulfate, proceeding via sulfite radicals (•SO_3^-) (Xu et al., 2024). In this pathway, a β-OSO_3^- alkoxy radical [-C(O•)–C(OSO_3^-)-] undergoes C–C bond cleavage, yielding an α-OSO_3^- alkyl radical, subsequently generating non-sulfate products and •SO_3^-. Upon the formation of •SO_4^- and •SO_3^-, inorganic sulfate can be formed through the further reactions of these radicals. In this study, the formation of inorganic sulfate ~~using UPLC~~during the reaction of phenyl sulfate with •OH was also examined. Figure S7a shows that the SO_4^{2-} peak in IC increased progressively with reaction time. The formation of inorganic sulfate was further supported by the evidence of the observed prominent HSO_4^- peak at *m/z* 97,

which is assigned to HSO_4^-, in the mass spectra (Fig. S6b), the intensity in the extracted ion chromatograms (EIC) was substantially higher than in dark controls (Fig. S8a), ruling out in-source fragmentation or hydrolysis as the source of HSO_4^-. The results of IC and mass spectrometry suggest that in addition to new OSs, ~~S6). Thus, the formation of~~ inorganic sulfate ~~is inferred~~can be formed during the reaction. The mechanism of inorganic sulfate formation is elucidated to be produced from the elimination of the sulfate group from phenyl sulfate, as well as the *ipso*-addition followed by disproportionation reaction as shown in Fig. 2. Phenyl sulfate can undergo *ipso*-addition to form OH-PS radical, the *ipso*-OH-adduct should either rapidly eliminate HSO_4^- ~~accompanying with the formation of phenoxyl radical (precursor of phenol),~~, or undergo bimolecular reactions with other isomers of the OH-PS radical to yield phenol upon elimination of HSO_4^- as well. However, compared to other OH addition pathways (o-add, m-add, and p-add), there is only very little room for the *ipso*-addition. It is noted that previous study has shown that benzoic acid can undergo decarboxylation reactions. (Singla et al., 2004). Another possible pathway for HSO_4^- production is proposed to occur via the elimination of the sulfate group from phenyl sulfate, as similar to the decarboxylation mechanism of benzoic acid. ~~Unexpectedly, the yield of inorganic sulfate was measured as >80% using IC (Fig. S7). Although the peak of inorganic sulfate in IC was negligible at the beginning of reactions, we still cannot establish that the peak of OS products in IC is not overlapped with the peak of inorganic sulfate. Thus, in this study, the yield of inorganic sulfate obtained from IC measurement is controversial, further investigation should be warranted. Nevertheless, the observation of inorganic sulfate in mass spectra for the first time implies that aromatic OSs can also be converted into inorganic sulfate in analogues to aliphatic Oss (Fig. S8).~~

~~We also examined the effects of pH value on the mechanism of reactions. Figure S9 reveals that $C_6H_5O_5S^-$ exists as three isomeric forms: ortho, meta, and para hydroxyphenyl sulfate, exhibiting distinct distribution patterns at different pH values. Additionally, the total abundance of $C_6H_5O_5S^-$ was significantly higher at pH 8 compared to pH 3. This finding aligns with previous work by Pan et al. (1993), which uncovered that the primary product of phenol from the reaction of benzene and the OH radical shows dramatically increased yields (up to 93%) under alkaline conditions (pH 12.3). The pH-dependent product distribution observed in our study also evidences that the reaction mechanism of phenyl sulfate with OH radicals is significantly influenced by solution pH.~~

~~Similar to phenyl sulfate, the oxidation of p-tolyl sulfate and 4-ethylphenyl sulfate by OH radicals primarily yields phenolic compounds through OH-addition pathways, along with the fragmented products and inorganic sulfates. However, the presence of additional alkyl substituents in p-tolyl sulfate and 4-ethylphenyl sulfate enables alternative reaction pathways, in which OH radicals can abstract hydrogen atoms, leading to the formation of aromatic alcohols and aldehydes. (Baltaretu et al., 2009; Liu et al., 2017; Forstner et al., 1997).~~

Tables S3 and S4 summarize the identified products from the liquid-phase reactions of p-tolyl sulfate and 4-ethylphenyl sulfate with •OH, respectively. The mechanisms of p-tolyl sulfate and 4-ethylphenyl sulfate oxidized by •OH are similar to that of phenyl sulfate as mentioned above. Similar to phenyl sulfate, the addition of •OH to the aromatic ring predominantly yields phenolic compounds, such as $C_7H_5O_5S^-$, $C_7H_7O_5S^-$, $C_8H_9O_5S^-$, and $C_8H_9O_6S^-$. Further oxidation initiated by hydrogen abstraction can also generate fragmented products, such as $C_5H_5O_6S^-$ and $C_4H_5O_7S^-$ (Tables S2 and S3). Moreover, the

presence of alkyl substituents for p-tolyl sulfate and 4-ethylphenyl sulfate can enable additional hydrogen abstraction pathways (Forstner et al., 1997; Baltaretu et al., 2009; Liu et al., 2017), leading to the formation of aromatic aldehydes (e.g., $C_7H_5O_5S^-$, $C_8H_7O_5S^-$). In addition to new OSs formed, the formation of inorganic sulfate was also observed during the process of either p-tolyl sulfate or 4-ethylphenyl sulfate oxidized by •OH. For p-tolyl sulfate, the gradual increase of the SO_4^{2-} peak with reaction time in IC as well as the pronounced signal of *m/z* 97 (HSO_4^-) observed in mass spectra provide robust evidences for the formation of inorganic sulfate during the reaction (Figs. S7b and S8b). For 4-ethylphenyl sulfate, SO_4^{2-} peak in IC was found to overlap with that of the compound itself (Fig. S7c). The inference that 4-ethylphenyl sulfate converts to inorganic sulfate is supported by comparing the intensity of HSO_4^- (*m/z* 97) peak of samples collected from illumination and dark conditions (Fig. S8c).

3.3 Optical property changes

Kinetic and mechanism results show that aromatic OSs can undergo rapid •OH oxidation to form a series of functionalized and fragmented compounds. ~~Previous studies reported that multiphase oxidation of aromatic organic compounds often induces significant alterations in the~~ The changes of optical properties ~~of the reaction system (Li et al., 2021; Arciva et al., 2024). Thus, the change of optical properties during the process of aromatic OSs reacting with OH radicals was also monitored. Figure 3 shows~~ resulting from the formation of these compounds were also investigated. Figure S9 shows the time-dependent absorption spectra of aromatic OSs during •OH oxidation at pH 3. As the reaction progressed, the consume of reactants accompanied with the increase in absorbance across 250–400 nm. ~~The enhanced~~To establish the relationship between light absorption ~~at 250–300 nm corresponds to $\pi \rightarrow \pi^*$ transitions, likely indicative of newly formed aromatic C=C and carbonyl (C=O) functional groups (Li et al., 2022; Tang et al., 2020). Meanwhile, the observation of remarkable~~and organic compounds, chromophores formed in the reaction were identified by correlating UV absorption ~~at 300–400 nm, absent in the reactants, suggests the formation of light-absorbing brown carbon (BrC) species (Harrison et al., 2020; Laskin and Nizkorodov, 2015). The multiphase reaction of aromatic OS with OH radical generates polyhydroxyl substitution products. The~~bands with the retention time based on UPLC-PAD-MS analysis. For phenyl sulfate, Figure 3a displays that phenyl sulfate (*m/z* 173) was the prominent chromophore with the retention time of 5.67–6.16 min at the beginning of the reaction, exhibiting a characteristic absorption peak at 262 nm (Fig. S9a). After the liquid-phase •OH oxidation, five major chromophores were observed as shown in Fig. 3c. Chromophore #4 was assigned to the unreacted phenyl sulfate. Figure 3c shows that Chromophore #1, #2, and #3 eluted at 3.47–3.72 min, 4.00–4.18 min, and 5.46–5.60 min, respectively. These newly formed chromophores exhibit red-shifted absorption peaks (Fig. 10a), likely due to the electron-donating effect of hydroxyl groups ~~elevates the~~increasing aromatic ring electron density ~~of the aromatic ring, inducing a redshift in the parent compound's absorption~~ (Hems and Abbatt, 2018). ~~Additionally, the generated BrC may originate from oligomers with large conjugated structures (Yu et al., 2014; Li et al., 2022). Although the three aromatic OSs~~ The results of EIC suggest that these chromophores correspond to co-eluting mixtures containing $C_6H_5O_5S^-$ isomers (*m/z* 189), along with $C_6H_5O_6S^-$ (*m/z* 205), $C_6H_5O_7S^-$ (*m/z* 221) and $C_6H_7O_8S^-$ (*m/z* 239) (Fig. 3d). Among these compounds, $C_6H_5O_6S^-$ exhibited ~~similar trends in UV-Vis spectral evolution,~~ the highest intensity.

Chromophore #5, eluting at 14.98–15.67 min, remained unidentified. Its later elution time suggests a larger molecular structure and lower polarity (Fleming et al., 2020). Additionally, there ~~are still differences. For instance, the p-tolyl sulfate showed the most pronounced absorption enhancement at 260 nm, while the absorption peak of 4-ethylphenyl sulfate at 260 nm undergoes a blue shift, which is related to the different substituents of the reaction products.~~

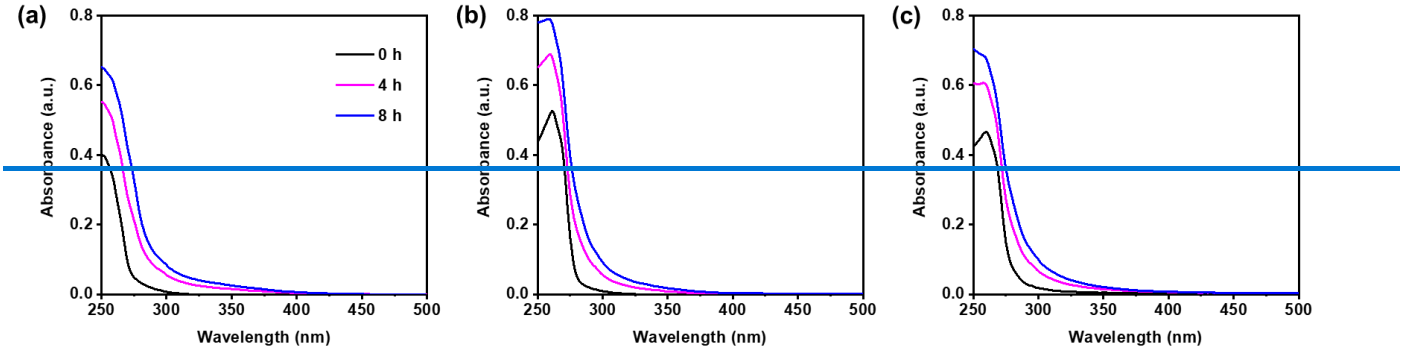

~~**Figure 3. The UV-vis**~~ may exist other chromophores unidentified since these five chromophores can not fully explain the total light ~~**absorption spectra of multiphase reaction of (a) phenyl sulfate, (b) p-tolyl sulfate and (c) 4-ethylphenyl sulfate with OH radical at pH 3.**~~adsorption as shown in Fig. 10a.

For p-tolyl sulfate, the increase in absorbance, contributing by the formation of chromophores, was also observed after OH oxidation. The primarily newly formed chromophore (Chromophore #1), eluting at 5.23–5.78 min, was identified as $C_7H_5O_5S^-$ (*m/z* 201) based on the corresponding EIC (Figs. S11c and d). A blue-shift peak at 258 nm was observed upon the formation of $C_7H_5O_5S^-$, which is associated with the generation of a carbonyl (C=O) functional group (Fig. S10b). Other newly formed chromophores were characterized as Chromophore #2 and Chromophore #3. Chromophore #2 corresponded to a mixture of $C_7H_7O_5S^-$ (*m/z* 203), $C_7H_7O_5S^-$ (*m/z* 217), and $C_7H_7O_6S^-$ (*m/z* 219) with absorption band at 274 nm, and Chromophore #3 was assigned to $C_7H_7O_5S^-$ (*m/z* 203) with the absorption band at 266 nm (Figs. S10b and S11). Figures S10c and S12 show the characterization of chromophores formed from liquid-phase reaction of 4-ethylphenyl sulfate with OH radicals. After reactions, Chromophore #2 ($C_8H_7O_5S^-$, *m/z* 215) with a characteristic absorption peak at 254 nm was the dominant contributor to total light absorption. Four additional chromophores were also identified: Chromophore #1, a mixture of $C_7H_7O_5S^-$ (*m/z* 201), $C_8H_9O_5S^-$ (*m/z* 217), $C_8H_7O_6S^-$ (*m/z* 231), and $C_8H_9O_6S^-$ (*m/z* 233), with absorption peak at 258 nm; Chromophore #3, an isomer of $C_8H_7O_6S^-$, with absorption peak at 262 nm; Chromophore #4, an isomer of $C_8H_9O_5S^-$ (*m/z* 217), with absorption peak at 274 nm; and Chromophore #5, another isomer of $C_8H_9O_5S^-$, also with a characteristic absorption peak at 274 nm.

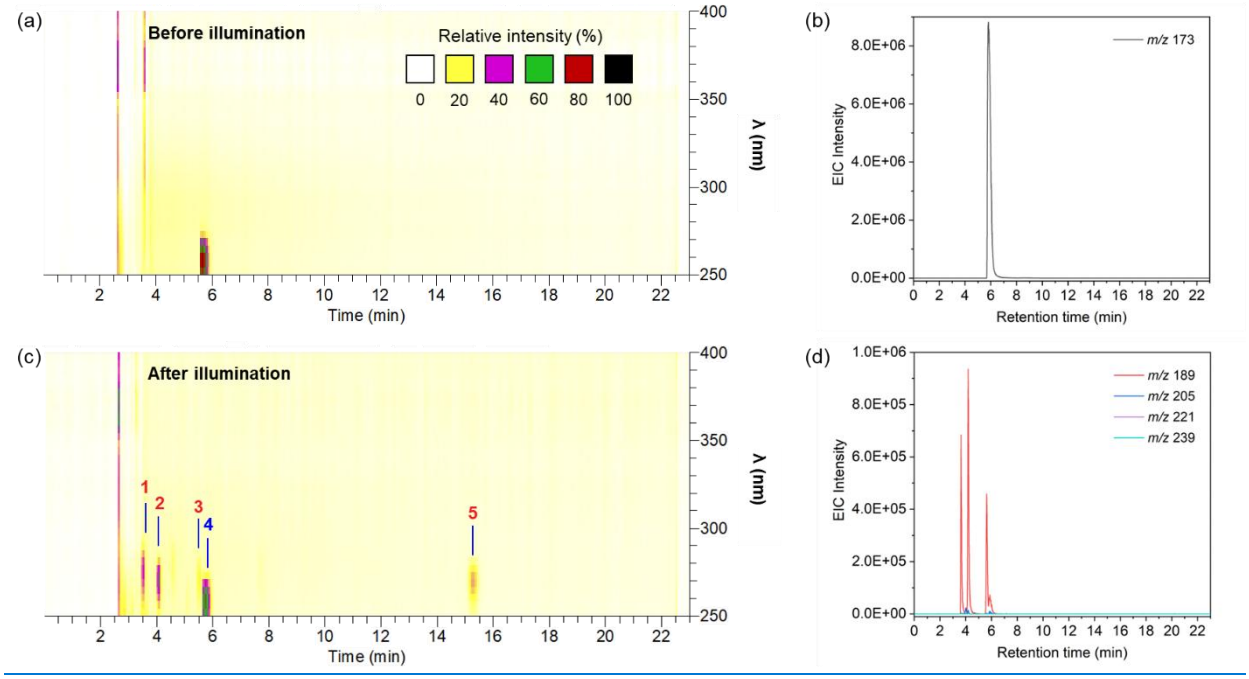

Figure 3. UPLC-PAD-MS chromatograms of samples collected (a) before and (c) after the liquid-phase •OH oxidation of phenyl sulfate at pH 3. The y-axis and color map represents the wavelength and corresponding UV-vis absorbance, respectively. Extracted ion chromatograms (EIC) of (b) phenyl sulfate and (d) the compositions of chromophores.

Furthermore, ~~the~~ fluorescence ~~characteristics of aromatic OSs~~ evolutions during ~~the multiphase~~liquid-phase •OH oxidation of aromatic OSs were investigated ~~using EEM fluorescence spectra. As~~as shown in Fig. 4. The initial maximum excitation/emission (Ex/Em) wavelengths of phenyl sulfate, p-tolyl sulfate, and 4-ethylphenyl sulfate at pH 3 were Ex/Em = 255/275 nm, 260/284 nm, and 260/284 nm, respectively. The different initial fluorescence intensity among these three aromatic OSs may be attributed to the substituent effect of the compound. Compared to phenyl sulfate, p-tolyl sulfate and 4-ethylphenyl sulfate contain additional methyl and ethyl groups, respectively. These electron-donating substituents extend the conjugation system, lowering the $\pi \rightarrow \pi^*$ transition energy and resulting in both emission redshift and fluorescence enhancement (Cao et al., 2023). During the reaction, the fluorescence intensity initially decreased due to phenyl sulfate consumption, followed by a subsequent increase from fluorescent product formation. After 8 h of illumination, a redshifted fluorescence peak emerged at Ex/Em = 260/283 nm, implying the formation of products with expanded conjugated systems (e.g., $C_6H_5O_5S^-$, $C_6H_5O_6S^-$ and $C_6H_5O_7S^-$) (Tang et al., 2020). The fluorescence intensity of p-tolyl sulfate and 4-ethylphenyl sulfate monotonically decreased with the reaction time and showed a redshift in the fluorescence band at Ex/Em = (250–300)/(400–500). Previous studies uncovered that the emission wavelengths of 400–500 nm are the indicative of humic-like substances (HULIS), which can significantly contribute to the light-absorbing properties of organic aerosols (Bianco et al., 2014). ~~In addition, when~~ Previous studies revealed that the oxidation of non-photolyzable ~~phenolic compounds are oxidized~~phenolics by •OH ~~yielding~~can yield HULIS-like fluorescent products (Tang et al., 2020; Chang et al., 2010). ~~with~~ Here, multi-hydroxy products from p-tolyl sulfate

(e.g., $C_7H_7O_5S^-$, $C_7H_7O_6S^-$ and $C_7H_7O_7S^-$) and 4-ethylphenyl sulfate (e.g., $C_8H_9O_5S^-$, $C_8H_9O_6S^-$ and $C_8H_9O_7S^-$) may exhibit spectral features resembling ~~those of~~ aerosol HULIS ~~(Tang, et al., .2020; Chang et al., 2010).~~

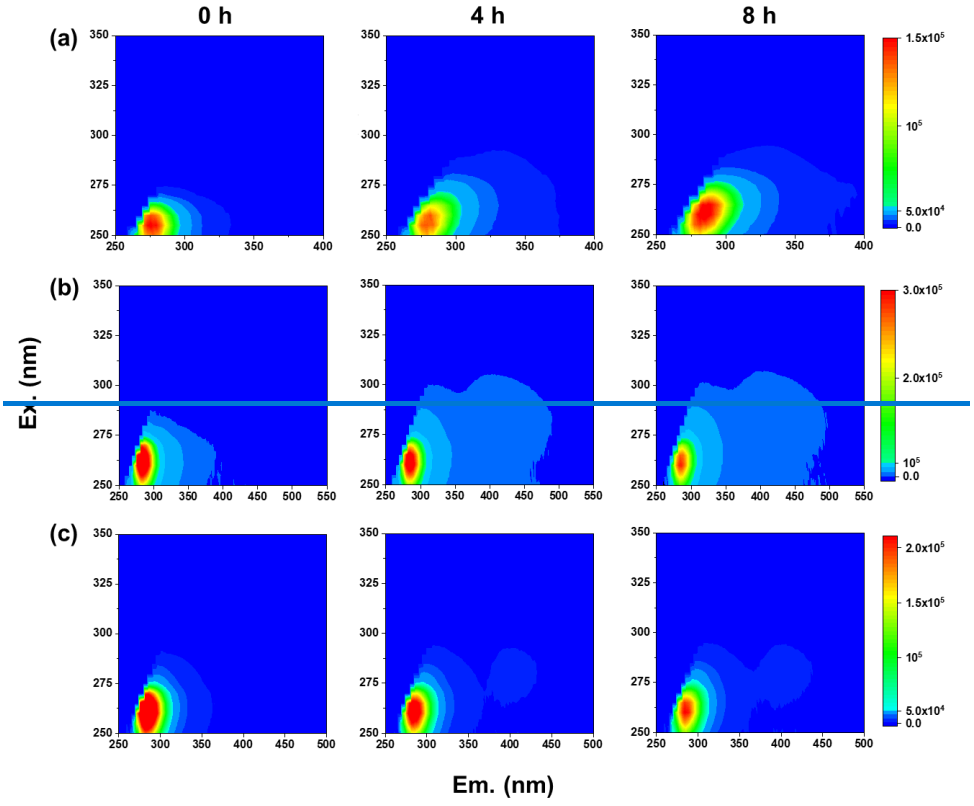

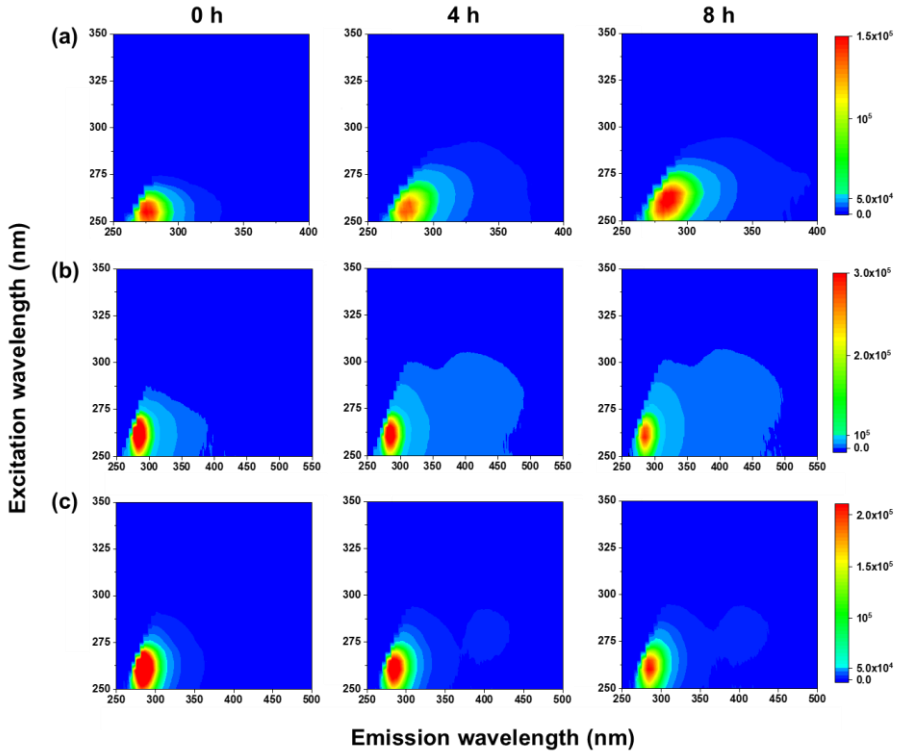

Figure 4. Time profile of excitation–emission matrix (EEM) fluorescence spectra during the processes of (a) phenyl sulfate, (b) p-tolyl sulfate and (c) 4-ethylphenyl sulfate reacting with •OH at pH 3.

Employing phenyl sulfate as the representative, ~~how the absorption spectra and EEM fluorescence spectra changed~~spectral changes at pH 8 were also examined. Previous studies have demonstrated that the light absorption properties of carbonyl compounds (e.g., aldehydes) and nitrophenols exhibit pronounced pH-dependence owing to protonation-deprotonation equilibria (Calvert and Schnitzler, 2023; Chen et al., 2020b). In this study, the phenyl sulfate remains deprotonated across the pH range of 3–8, resulting in negligible spectral variations in the initial solution (Figs. S9 and S13). However, the temporal evolution of the reaction revealed substantially enhanced absorbance at pH 3 compared to pH 8, particularly within the 300–400 nm range. ~~This pronounced difference suggests that low pH preferentially facilitates~~Figure S14 shows the ~~formation~~molecular composition of ~~light-absorbing BrC species, likely through acid-catalyzed oligomerization (Heath and Valsaraj, 2013). Figure S11 reveals that~~ chromophores from the reaction of phenyl sulfate ~~exhibits~~with •OH at pH 8. Chromophores #1–3 were identical to those at pH 3 but exhibited stronger absorption due to their higher concentrations. An additional chromophore #4, eluting at 4.99–5.23 min, contributed significantly to absorption but the detailed composition of this chromophore is unknown. Compared to pH 3, solution of pH 8 exhibited an enhanced peak intensity at 4.99–5.23 min, while the peak at 14.98–15.67 min was reduced, which corresponded to distinct changes in the relative contributions to total absorption. For fluorescence spectra, phenyl sulfate exhibited an initial maximum fluorescence peak at Ex/Em = 255/279 nm at pH 8~~, showing~~ (Fig. S15), displaying minimal variation from the pH 3 conditions (Fig. 4a). However, the temporal evolution

of its fluorescence spectrum differs obviously at different pH values. Under basic conditions (pH 8), ~~we observed a monotonic decrease in~~ fluorescence ~~intensity~~decreased monotonically without ~~subsequent~~ recovery, and no ~~fluorescence peak redshift~~red shift occurred even after 8 ~~hours of reaction. This pH-dependent fluorescence behavior suggests distinct oxidation pathways under acidic versus basic conditions. The pronounced fluorescence redshift observed exclusively under acidic conditions further implies that larger, more conjugated photoproducts form preferentially under acidic conditions~~h.

4 Atmospheric implications and conclusions

The current study ~~investigates~~investigated the ~~multiphase~~liquid-phase reactions of three aromatic OSs (i.e., phenyl sulfate, p-tolyl sulfate, and ~~OH radicals.~~4-ethylphenyl sulfate) with •OH. It is found that functionalized and fragmented OSs as well as inorganic sulfate can be yielded during the reactions. The formation of functionalized OSs can enhance light absorption, thereby influencing aerosol optical properties. Fragmented OS formation resulting from ring-opening pathways during •OH oxidation of aromatic OSs has not reported previously. Several fragmented OSs (e.g., $C_2H_3O_5S^-$, $C_5H_7O_8S^-$, $C_4H_5O_7S^-$, and $C_5H_5O_6S^-$) detected in our study have been previously identified in ambient aerosols (Kuang et al., 2016; Cai et al., 2020; Wang et al., 2022; Yang et al., 2023), suggesting that aromatic OSs may serve as a potential source for aliphatic OSs in the atmosphere. Furthermore, the observation of inorganic sulfate formation, for the first time, indicates that aromatic OSs can also be converted into inorganic sulfate in analogy to aliphatic OSs (Kwong et al., 2018; Xu et al., 2022, 2024; Lai et al., 2025), potentially contributing to the atmospheric sulfur cycle. Further investigations are warranted to examine whether the proposed mechanism can be also applied to other types of aromatic OSs in the atmosphere.

The results of kinetic measurements ~~indicate~~reveal that aromatic OSs can ~~undergo multiple reactions with OH radicals~~react rapidly with •OH. As shown in Table S5, using the k values coupled with modeled •OH concentrations (Herrmann et al., 2005, 2010), the corresponding lifetimes ($\tau=1/k_{OS}\times[\bullet OH]$) of aromatic OSs can be calculated. In urban ~~aerosol and~~areas, the concentrations of •OH in cloud ~~was calculated to be 7 minutes and 16 h~~and aerosol are estimated as 3.5×10^{-15} and 4.4×10^{-13} M, respectively. ~~The lifetime of aromatic OSs is significantly shorter than those of aliphatic OSs~~ In contrast to urban areas, remote areas exhibit higher •OH concentrations both in cloud (2.2×10^{-14} M) and aerosol (3.0×10^{-12} M) (Herrmann et al., 2005, 2010). Concentrations of •OH are consistently higher in aerosol than in cloud water across different environments. Consequently, the lifetimes of aromatic OSs range from approximately 1 min in remote aerosols to up to 16 h in urban cloud water (Table S5), highlighting the significant influence of environmental conditions on their persistence. Previous studies reported that the lifetimes of aliphatic OSs in such varied environments range from several minutes to dozen days (Gweme and Styler, 2024; Lai et al., ~~2025). The formed aromatics OSs can be transformed into functionalized and fragmented OSs as well as inorganic sulfates. Notably, the detection of alkyl OSs in the oxidation products challenges the conventional attribution of these compounds solely to biological sources, revealing aromatic OSs as an additional precursor in the atmosphere. Furthermore, the multiphase reaction of aromatic OSs with OH radicals generates functionalized OSs, which act as a BrC component to enhance light absorption, thereby influencing aerosol optical properties and perturbing radiative forcing. The~~

2025). The substantially shorter lifetimes of aromatic OSs can be attributed to their higher reactivity toward OH radicals compared to aliphatic OSs. Given the high abundance ~~and short atmospheric lifetime~~ of aromatic OSs and their fast reactivity with •OH in urban environments ~~further underscores their potentially~~, aromatic OSs likely play a significant role in both the atmospheric sulfur cycle and environmental effects. ~~These findings establish that the multiphase reaction of aromatic OS with OH radical is a key transformation pathway and emphasize the significant impact of this pathway on urban aerosol chemistry and related climate effects.~~In addition to lifetimes in aqueous environments, previous studies also estimated the atmospheric lifetimes of several aliphatic OSs via heterogeneous •OH oxidation based on measured uptake coefficients (Kwong et al., 2018; Lam et al., 2019; Xu et al., 2022). For instance, the atmospheric lifetime of methyl sulfate ranges from 53 min to 32 days via liquid-phase OH radical oxidation, compared to approximately 20 days via heterogeneous •OH oxidation (Gweme and Styler, 2024; Kwong et al., 2018). The results indicate that the atmospheric lifetimes of these OSs differ between liquid-phase and heterogeneous •OH oxidation pathways. However, experiments of heterogeneous reactions of aromatic OSs with •OH were not conducted in this study. Thus, we cannot directly compare the lifetime of aromatic and aliphatic OSs through heterogeneous •OH oxidation, and need further investigations.

Data availability. Data are available upon request from the corresponding author.

Supplement. The supplement related to this article is available online.

Author contributions. LH designed research. YY, CY RY, PL, HZ, and HC, performed research. YY and LH analyzed data. YY and LH wrote the paper. LX, CY, YW, YZ, and HS provided valuable comments and suggestions for the manuscript.

Competing interests. The contact author has declared that none of the authors has any competing interests.

Acknowledgements. This study was financially supported by the National Key Research and Development Program of China (2022YFC3701102), the National Natural Science Foundation of China (42207121), the Outstanding Young Scholar of the Natural Science Foundation of Shandong Province, China (Overseas) (2022HWYQ-010), the Natural Science Foundation of Shandong Province (ZR2024YQ046). Liubin Huang gratefully acknowledges the support of the Program for Taishan Young Scholar (tsqnz20221107).

References

Arciva, S., Niedek, C., Mavis, C., Yoon, M., Sanchez, M. E., Zhang, Q., and Anastasio, C.: Aqueous ·OH oxidation of highly substituted phenols as a source of secondary organic aerosol, Environ. Sci. Technol., 56, 9959–9967, https://doi.org/10.1021/acs.est.2c02225, 2022.

Arciva, S., Ma, L., Mavis, C., Guzman, C., and Anastasio, C.: Formation and loss of light absorbance by phenolic aqueous SOA by •OH and an organic triplet excited state, Atmos. Chem. Phys., 24, 4473–4485, https://doi.org/10.5194/acp-24-4473-2024, 2024.

Armstrong, N. C.; Chen, Y.; Cui, T.; Zhang,Y.; Christensen, C.; Zhang, Z.; Turpin, B. J.; Chan, M. N.; Gold, A.; Ault, A. P. Isoprene epoxydiol-derived sulfated and nonsulfated oligomers suppress particulate mass loss during oxidative aging of secondary organic aerosol. Environ. Sci.Technol. 2022, 56, 16611.

Baltaretu, C. O., Lichtman, E. I., Hadler, A. B., and Elrod, M. J.: Primary atmospheric oxidation mechanism for toluene, J. Phys. Chem. A, 113, 221–230, https://doi.org/10.1021/jp806841t, 2009.

Bianco, A., Minella, M., Laurentiis, E. D., Maurino, V., Minero, C., and Vione, D.: Photochemical generation of photoactive compounds with fulvic-like and humic-like fluorescence in aqueous solution, Chemosphere, 111, 529–536, https://doi.org/10.1016/j.chemosphere.2014.04.035, 2014.

Bloss, C., Wagner, V., Jenkin, M. E., Volkamer, R., Bloss, W. J., Lee, J. D., Heard, D. E., Wirtz, K., Martin-Reviejo, M., Rea, G., Wenger, J. C., and Pilling, M. J.: Development of a detailed chemical mechanism (MCMv3.1) for the atmospheric oxidation of aromatic hydrocarbons, Atmos. Chem. Phys., 5, 641–664, https://doi.org/10.5194/acp-5-641-2005, 2005.

Buxton, G. V., Greenstock, C. L., Helman, W. P., and Ross, A. B.: Critical review of rate constants for reactions of hydrated electrons, hydrogen atoms and hydroxyl radicals (•OH/•O− in aqueous solution, J. Phys. Chem. Ref. Data, 17, 513–886, https://doi.org/10.1063/1.555805, 1988.

Cai, D., Wang, X., Chen, J., and Li, X.: Molecular characterization of organosulfates in highly polluted atmosphere using ultra-high-resolution mass spectrometry, J GEOPHYS RES-ATMOS, 125, e2019JD032253, https://doi.org/10.1029/2019JD032253, 2020.

Calvert, C. T., and Schnitzler, E. G.: Light absorption by cinnamaldehyde constituents of biomass burning organic aerosol modeled using time-dependent density functional theory, ACS Earth Space Chem, 7, 490–500, https://doi.org/10.1021/acsearthspacechem.2c00344, 2023.

Cao, T., Li, M., Xu, C., Song, J., Fan, X., Li, J., Jia, W., and Peng, P.: Technical note: Chemical composition and source identification of fluorescent components in atmospheric water-soluble brown carbon by excitation–emission matrix spectroscopy with parallel factor analysis – potential limitations and applications, Atmos. Chem. Phys., 23, 2613–2625, https://doi.org/10.5194/acp-23-2613-2023, 2023.

Chang, J. L., and Thompson, J. E.: Characterization of colored products formed during irradiation of aqueous solutions containing H_2O_2 and phenolic compounds, Atmos. Environ., 44, 541–551,

https://doi.org/10.1016/j.atmosenv.2009.10.042, 2010.

Chen, Y., Zhang, Y., Lambe, A. L., Xu, R., Lei, Z., Olson, N. E., Zhang, Z., Szalkowski, T., Cui, T., Vizuete, W., Gold, A., Turpin, B. J., Ault, A. P., Chan, M. N., Surratt, J. D.: Heterogeneous hydroxyl radical oxidation of isoprene-epoxydiol-derived methyltetrol sulfates: Plausible formation mechanisms of previously unexplained organosulfates in ambient fine aerosols, Environ. Sci. Technol. Lett., 7, 460–468, https://doi.org/10.1021/acs.estlett.0c00276, 2020a.

Chen, J. Y., Rodriguez, E., Jiang, H., Chen, K., Frie, A., Zhang, H., Bahreini, R., and Lin, Y-H.: Time-dependent density functional theory investigation of the UV–Vis spectra of organonitrogen chromophores in brown carbon, ACS Earth Space Chem., 4, 311–320, https://doi.org/10.1021/acsearthspacechem.9b00328, 2020b.

Darer, A. I., Cole-Filipiak, N. C., O'Connor, A. E., and Elrod, M. J.: Formation and stability of atmospherically relevant isoprene-derived organosulfates and organonitrates, Environ. Sci. Technol., 45, 1895–1902, https://doi.org/10.1021/es103797z, 2011.

Dong, P., Chen, Z., Qin, X., and Gong, Y.: Water significantly changes the ring-cleavage process during aqueous photooxidation of toluene, Environ. Sci. Technol., 55, 16316–16325, https://doi.org/10.1021/acs.est.1c04770, 2021.

Dorfman, L. M., and Adams, G. E.: Reactivity of the hydroxyl radical in aqueous solutions, National Bureau of Standards, 76, 1973.

Forstner, H. J. L., Flagan, R. C., and Seinfeld, J. H.: Secondary organic aerosol from the photooxidation of aromatic hydrocarbons: Molecular composition, Environ. Sci. Technol., 31, 1345–1358, https://doi.org/10.1021/es9605376, 1997.

Garmash, O., Rissanen, M. P., Pullinen, I., Schmitt, S., Kausiala, O., Tillmann, R., Zhao, D., Percival, C., Bannan, T. J., Priestley, M., Hallquist, Å. M., Kleist, E., Kiendler-Scharr, A., Hallquist, M., Berndt, T., McFiggans, G., Wildt, J., Mentel, T. F., and Ehn, M.: Multi-generation OH oxidation as a source for highly oxygenated organic molecules from aromatics, Atmos. Chem. Phys., 20, 515–537, https://doi.org/10.5194/acp-20-515-2020, 2020.

Gweme, D. T., and Styler, S. A.: OH radical oxidation of organosulfates in the atmospheric aqueous phase, J. Phys. Chem. A, 128, 9462–9475, https://doi.org/10.1021/acs.jpca.4c02877, 2024.

Hansen, A. M. K., Kristensen, K., Nguyen, Q. T., Zare, A., Cozzi, F., Nøjgaard, J. K., Skov, H., Brandt, J., Christensen, J. H., Ström, J., Tunved, P., Krejci, R., and Glasius, M.: Organosulfates and organic acids in Arctic aerosols: speciation, annual variation and concentration levels, Atmos. Chem. Phys., 14, 7807–7823, https://doi.org/10.5194/acp-14-7807-2014, 2014.

Harrison, A. W., Waterson, A. M., and De Bruyn, W. J.: Spectroscopic and photochemical properties of secondary brown carbon from aqueous reactions of methylglyoxal, ACS Earth Space Chem., 4, 762–773, https://doi.org/10.1021/acsearthspacechem.0c00061, 2020.

He, J., Li, L., Li, Y., Huang, M., Zhu, Y., and Deng, S.: Synthesis, MS/MS characteristics and quantification of six aromatic organosulfates in atmospheric $PM_{2.5}$, Atmos. Environ., 290, 119361, https://doi.org/10.1016/j.atmosenv.2022.119361, 2022.

Heath, A. A., Ehrenhauser, F. S., and Valsaraj, K. T.: Effects of temperature, oxygen level, ionic strength, and pH on the reaction of benzene with hydroxyl radicals in aqueous atmospheric systems, Environ. Chem. Eng., 1, 822–830,

https://doi.org/10.1016/j.jece.2013.07.023, 2013.

Hems, R. F., and Abbatt, J. P. D.: Aqueous phase photo-oxidation of brown carbon nitrophenols: Reaction kinetics, mechanism, and evolution of light absorption, ACS Earth Space Chem., 2, 225–234, https://doi.org/10.1021/acsearthspacechem.7b00123, 2018.

Herrmann, H., Schaefer, T., Tilgner, A., Styler, S. A., Weller,C., Teich, M., and Otto, T.: Tropospheric aqueous-phase chemistry: kinetics, mechanisms, and its coupling to a changing gas phase, Chem. Rev., 115, 4259–4334, https://doi.org/10.1021/cr500447k, 2015.

Herrmann, H., Tilgner, A., Barzaghi, P., Majdik, Z., Gligorovski, S., Poulain, L., and Monod, A.: Towards a more detailed description of tropospheric aqueous phase organic chemistry: CAPRAM 3.0, Atmos. Environ., 39, 4351–4363, https://doi.org/10.1016/j.atmosenv.2005.02.016, 2005.

Herrmann, H., Hoffmann, D., Schaefer, T., Bräuer, P., and Tilgner, A.: Tropospheric aqueous-phase free-radical chemistry: Radical sources, spectra, reaction kinetics and prediction tools, ChemPhysChem, 11, 3796–3822, https://doi.org/10.1002/cphc.201000533, 2010.

Hettiyadura, A. P. S., Al-Naiema, I. M., Hughes, D. D., Fang, T., and Stone, E. A.: Organosulfates in Atlanta, Georgia: anthropogenic influences on biogenic secondary organic aerosol formation, Atmos. Chem. Phys., 19, 3191–3206, https://doi.org/10.5194/acp-19-3191-2019, 2019.

Hettiyadura, A. P. S., Jayarathne, T., Baumann, K., Goldstein, A. H., de Gouw, J. A., Koss, A., Keutsch, F. N., Skog, K., and Stone, E. A.: Qualitative and quantitative analysis of atmospheric organosulfates in Centreville, Alabama, Atmos. Chem. Phys., 17, 1343–1359, https://doi.org/10.5194/acp-17-1343-2017, 2017.

Hu, K. S., Darer, A. I., and Elrod, M. J.: Thermodynamics and kinetics of the hydrolysis of atmospherically relevant organonitrates and organosulfates, Atmos. Chem. Phys., 11, 8307–8320, https://doi.org/10.5194/acp-11-8307-2011, 2011.

Hu, W. W., Campuzano-Jost, P., Palm, B. B., Day, D. A., Ortega, A. M., Hayes, P. L., Krechmer, J. E., Chen, Q., Kuwata, M., Liu, Y. J., de Sá, S. S., McKinney, K., Martin, S. T., Hu, M., Budisulistiorini, S. H., Riva, M., Surratt, J. D., St. Clair, J. M., Isaacman-Van Wertz, G., Yee, L. D., Goldstein, A. H., Carbone, S., Brito, J., Artaxo, P., de Gouw, J. A., Koss, A., Wisthaler, A., Mikoviny, T., Karl, T., Kaser, L., Jud, W., Hansel, A., Docherty, K. S., Alexander, M. L., Robinson, N. H., Coe, H., Allan, J. D., Canagaratna, M. R., Paulot, F., and Jimenez, J. L.: Characterization of a real-time tracer for isoprene epoxydiols-derived secondary organic aerosol (IEPOX-SOA) from aerosol mass spectrometer measurements, Atmos. Chem. Phys., 15, 11807–11833, https://doi.org/10.5194/acp-15-11807-2015, 2015.

Huang, L., Cochran, R. E., Coddens, E. M., and Grassian, V. H.: Formation of organosulfur compounds through transition metal ion-catalyzed aqueous phase reactions, nviron. Sci. Technol. Lett., 5, 315–321, https://doi.org/10.1021/acs.estlett.8b00225, 2018.

Huang, L., Wang, Y., Zhao, Y., Hu, H., Yang, Y., Wang, Y., Yu, J-Z., Chen, T., Cheng, Z., Li, C., and Xiao., H.: Biogenic and anthropogenic contributions to atmospheric organosulfates in a typical megacity in eastern China, J GEOPHYS RES-ATMOS, 128, e2023JD038848, https://doi.org/10.1029/2023JD038848, 2023.

Iinuma, Y., Müller, C., Berndt, T., Böge, O., Claeys, M., and Herrmann, H.: Evidence for the existence of organosulfates from β-Pinene ozonolysis in ambient secondary organic aerosol, Environ. Sci. Technol., 41, 6678–6683, https://doi.org/10.1021/es070938t, 2007.

Kuang, B. Y., Lin, P., Hu, M., and Yu, J., Z.: Aerosol size distribution characteristics of organosulfates in the Pearl River Delta region, China, Atmos. Environ.,130, 23–35, https://doi.org/10.1016/j.atmosenv.2015.09.024, 2016.

Kundu, S., Quraishi, T. A., Yu, G., Suarez, C., Keutsch, F. N., and Stone, E. A.: Evidence and quantitation of aromatic organosulfates in ambient aerosols in Lahore, Pakistan, Atmos. Chem. Phys., 13, 4865–4875, https://doi.org/10.5194/acp-13-4865-2013, 2013.

Kwong, K. C., Chim, M. M., Davies, J. F., Wilson, K. R., and Chan, M. N.: Importance of sulfate radical anion formation and chemistry in heterogeneous •OH oxidation of sodium methyl sulfate, the smallest organosulfate, Atmos. Chem. Phys., 18, 2809–2820, https://doi.org/10.5194/acp-18-2809-2018, 2018.

Kristensen, K., and Glasius, M.: Organosulfates and oxidation products from biogenic hydrocarbons in fine aerosols from a forest in north west Europe during spring, Atmos. Environ., 45, 4546–4556, https://doi.org/10.1016/j.atmosenv.2011.05.063, 2011.

Lai, D., Schaefer, T., Zhang, Y., Li, Y. J., Xing, S., Herrmann, H., and Chan, M. N.: Deactivating effect of hydroxyl radicals reactivity by sulfate and sulfite functional groups in aqueous phase─atmospheric implications for small organosulfur compounds, ACS EST Air, 1, 678–689, https://doi.org/10.1021/acsestair.4c00033, 2024.

Lai, D., Bai, Y., Zhang, Z., So, P.-K., Li, Y. J., Tse, Y.-L. S., Yeung, Y.-Y., Schaefer, T., Herrmann, H., Yu, J. Z., Wang, Y., and Chan, M. N.: Rapid aqueous-phase oxidation of an α-pinene-derived organosulfate by hydroxyl radicals: a potential source of some unclassified oxygenated and small organosulfates in the atmosphere, Atmos. Chem. Phys., 25, 12569–12584, https://doi.org/10.5194/acp-25-12569-2025, 2025.

Laskin, A., Laskin, J., and Nizkorodov, S. A.: Chemistry of atmospheric brown carbon, Chem. Rev., 115, 4335–4382, https://doi.org/10.1021/cr5006167, 2015.

Lay., T. H., Bozzelli, J. W., and Seinfeld, J. H.: Atmospheric photochemical oxidation of benzene: benzene + OH and the benzene−OH adduct (hydroxyl-2,4-cyclohexadienyl) + O_2, J. Phys. Chem., 100, 6543–6554, https://doi.org/10.1021/jp951726y, 1996.

Lei, Z., Chen, Y.., Zhang, Y., Cooke, M. E., Ledsky, I. R., Armstrong, N. C., Olson, N. E., Zhang, Z., Gold, A., Surratt, J. D., and Ault, A. P.: Initial pH governs secondary organic aerosol phase state and morphology after uptake of isoprene epoxydiols (IEPOX), Environ. Sci. Technol., 56, 10596–10607, https://doi.org/10.1021/acs.est.2c01579, 2022.

Li, F., Tsona, N. T., Li, J., and Du, L.: Aqueous-phase oxidation of syringic acid emitted from biomass burning: Formation of light-absorbing compounds, Sci. Total Environ., 765, 144239, https://doi.org/10.1016/j.scitotenv.2020.144239, 2021.

Li, S., Wang, Y., Zhang, Y., Yi, Y., Wang, Y., Guo, Y., Yu, C., Jiang, Y., Shi, J., Zhang, C., Zhu, J., Hu, W., Yu, J., Yao, X., Gao, H., and Hu, M.: Atmospheric organosulfate formation regulated by continental outflows and marine emissions over East Asian marginal seas, Atmos. Chem. Phys., 25, 12585–12598, https://doi.org/10.5194/acp-25-12585-2025, 2025.

Li, X., Tao, Y., Zhu, L.,Ma, S., Luo, S., Zhao, Z., Sun, N., Ge, X., and Ye, Z.: Optical and chemical properties and oxidative potential of aqueous phase products from •OH and 3C* initiated photooxidation of eugenol, Atmos. Chem. Phys., 22, 7793–7814, https://doi.org/10.5194/acp-22-7793-2022, 2022.

Liu, F., Xu, T., Ng, N. L., and Lu, H.: Linking cell health and reactive oxygen species from secondary organic aerosols exposure, Environ. Sci. Technol., 57, 1039–1048, https://doi.org/10.1021/acs.est.2c05171, 2022.

Liu, G., Ji, J., Huang, H., Xie, R., Feng, Q., Shu, Y., Zhan, Y., Fang, R., He, M., Liu, S., Ye, X., and Leung, D. Y. C.: UV/H_2O_2: An efficient aqueous advanced oxidation process for VOCs removal, Chem. Eng. J., 324, 44–50, https://doi.org/10.1016/j.cej.2017.04.105, 2017.

Lin, Y.-H., Knipping, E. M., Edgerton, E. S., Shaw, S. L., and Surratt, J. D.: Investigating the influences of SO_2 and NH_3 levels on isoprene-derived secondary organic aerosol formation using conditional sampling approaches, Atmos. Chem. Phys., 13, 8457–8470, https://doi.org/10.5194/acp-13-8457-2013, 2013.

Lukács, H., Gelencsér, A., Hoffer, A., Kiss, G., Horváth, K., and Hartyáni, Z.: Quantitative assessment of organosulfates in size-segregated rural fine aerosol, Atmos. Chem. Phys., 9, 231–238, https://doi.org/10.5194/acp-9-231-2009, 2009.

Ma, J., Reininger, N., Zhao, C, Döbler, D., Rüdiger, J., Qiu, Y., Ungeheuer, F., Simon, M., D'Angelo, L., Breuninger, A., David, J., Bai, Y., Li, Y., Xue, Y., Li, L., Wang, Y., Hildmann, S., Hoffmann, T., Liu, B., Niu, H., Wu, Z., and Vogel, A. L.: Unveiling a large fraction of hidden organosulfates in ambient organic aerosol, Nat. Commun., 16, 4098, https://doi.org/10.1038/s41467-025-59420-y, 2025.

Ma, Y., Xu, X., Song, W., Geng, F., and Wang, L.: Seasonal and diurnal variations of particulate organosulfates in urban Shanghai, China, Atmos. Environ., 85, 152–160, https://doi.org/10.1016/j.atmosenv.2013.12.017, 2014.

Mael, L. E., Jacobs, M. I., and Elrod, M. J.: Organosulfate and nitrate formation and reactivity from epoxides derived from 2-Methyl-3-buten-2-ol, J. Phys. Chem. A, 119, 4464–4472, https://doi.org/10.1021/jp510033s, 2015.

Minakata, D., Song, W., Mezyk, S. P., and Cooper, W. J.: Experimental and theoretical studies on aqueous-phase reactivity of hydroxyl radicals with multiple carboxylated and hydroxylated benzene compounds, Phys. Chem. Chem. Phys., 17, 11796–11812, https://doi.org/10.1039/C5CP00861A, 2015.

Minerath, E. C., Casale, M. T., and Elrod, M. J.: Kinetics feasibility study of alcohol sulfate esterification reactions in tropospheric aerosols, Environ. Sci. Technol., 42, 4410–4415, https://doi.org/10.1021/es8004333, 2008.

Monod, A., and Doussin, J. F.: Structure-activity relationship for the estimation of OH-oxidation rate constants of aliphatic organic compounds in the aqueous phase: alkanes, alcohols, organic acids and bases, Atmos. Environ., 42, 7611-7622, https://doi.org/10.1016/j.atmosenv.2008.06.005, 2008.

Nozière, B., Ekström, S., Alsberg, T., and Holmström S.: Radical-initiated formation of organosulfates and surfactants in atmospheric aerosols, Geophys. Res. Lett., 37, L05806, https://doi.org/10.1029/2009GL041683, 2010.

Pan, X-M., Schuchmann, M. N., and Sonntag, C. V.: Oxidation of benzene by the OH radical. A product and pulse radiolysis study in oxygenated aqueous solution, J. Chem. Soc., Perkin Trans., 2, 289–297, https://doi.org/10.1039/P29930000289, 1993.

Passananti, M., Kong, L., Shang, J., Dupart, Y., Perrier, S., Chen, J., Donaldson, J., and George, C.: Organosulfate formation through the heterogeneous reaction of sulfur dioxide with unsaturated fatty acids and long-chain alkenes, Angew. Chem. Int. Ed., 55, 10336-10339, https://doi.org/10.1002/anie.201605266, 2016.

Peng, X., Xie, T-T., Tang, M-X., Cheng, Y., Peng, Y., Wei, F-H., Cao, L-M., Yu, K., Du, K., He, L-Y., and Huang, X-F.: Critical role of secondary organic aerosol in urban atmospheric visibility improvement identified by machine learning, Environ. Sci. Technol. Lett., 10, 976–982, https://doi.org/10.1021/acs.estlett.3c00084, 2023.

Pye, H. O. T., Nenes, A., Alexander, B., Ault, A. P., Barth, M. C., Clegg, S. L., Collett Jr., J. L., Fahey, K. M., Hennigan, C. J., Herrmann, H., Kanakidou, M., Kelly, J. T., Ku, I.-T., McNeill, V. F., Riemer, N., Schaefer, T., Shi, G., Tilgner, A., Walker, J. T., Wang, T., Weber, R., Xing, J., Zaveri, R. A., and Zuend, A.: The acidity of atmospheric particles and clouds, Atmos. Chem. Phys., 20, 4809–4888, https://doi.org/10.5194/acp-20-4809-2020, 2020.

Riva, M., Chen, Y., Zhang, Y., Lei, Z., Olson, N. E., Boyer, H. C., Narayan, S., Yee, L. D., Green, H. S., Cui, T., Zhang, Z., Baumann, K., Fort, M., Edgerton, E., Budisulistiorini, S. H., Rose, C. A., Ribeiro, I. O., e Oliveira, R. L., dos Santos, E. O., Machado, C. M. D., Szopa, S., Zhao, Y., Alves, E. G., de Sá, S. S., Hu, W., Knipping, E. M., Shaw, S. L., Junior, S. D., de Souza, R. A. F., Palm, B. B., Jimenez, J-L., Glasius, M., Goldstein, A. H., Pye, H. O. T., Gold, A., Turpin, B. J., Vizuete, W., Martin, S. T., Thornton, J. A., Dutcher, C. S., Ault, A. P., and Surratt, J. D.: Increasing isoprene epoxydiol-to-inorganic sulfate aerosol ratio results in extensive conversion of inorganic sulfate to organosulfur forms: Implications for aerosol physicochemical properties, Environ. Sci. Technol., 53, 8682–8694, https://doi.org/10.1021/acs.est.9b01019, 2019.

Schindelka, J., Iinuma, Y., Hoffmann, D., and Herrmann, H.: Sulfate radical-initiated formation of isoprene-derived organosulfates in atmospheric aerosols, Faraday Discuss., 165, 237–259, https://doi.org/10.1039/C3FD00042G, 2013.

Schuler, R. H., and Albarran, G.: The rate constants for reaction of radical •OH radicals with benzene and toluene, Radiat. Phys. Chem., 64, 189–195, https://doi.org/10.1016/S0969-806X(01)00497-2, 2002.

Shang, J., Passananti, M., Dupart, Y., Ciuraru, R., Tinel, L., Rossignol, S., Perrier, S., Zhu, T., and George, C.: SO_2 uptake on oleic acid: A new formation pathway of organosulfur compounds in the atmosphere, Environ. Sci. Technol. Lett., 3, 67–72, https://doi.org/10.1021/acs.estlett.6b00006, 2016.

Shrivastava, M., Cappa, C. D., Fan, J., Goldstein, A. H., Guenther, A. B., Jimenez, J. L., Kuang, C., Laskin, A., Martin, S. T., Ng, N. L., Petaja, T., Pierce, J. R., Rasch, P. J., Roldin, P., Seinfeld, J. H., Shilling, J., Smith, J. N., Thornton, J. A., Volkamer, R., Wang, J., Worsnop, D. R., Zaveri, R. A., Zelenyuk, A., and Zhang, Q.: Recent advances in understanding secondary organic aerosol: Implications for global climate forcing, Rev. Geophys., 55, 509–559, https://doi.org/10.1002/2016RG000540, 2017.

Singla, R., Ashokkumar, M., and Grieser, F.: The mechanism of the sonochemical degradation of benzoic acid in aqueous solutions, Res. Chem. Intermed., 30, 723–733, https://doi.org/10.1163/1568567041856963, 2004.

Smith, J. D., Kinney, H., and Anastasio, C.: Aqueous benzene-diols react with an organic triplet excited state and hydroxyl radical to form secondary organic aerosol, Phys. Chem. Chem. Phys., 17, 10227–10237,

https://doi.org/10.1039/C4CP06095D, 2015.

Surratt, J. D., Gómez-González, Y., Chan, A. W. H., Vermeylen, R., Shahgholi, M., Kleindienst, T. E., Edney, E. O., Offenberg, J. H., Lewandowski, M., Jaoui, M., Maenhaut, W., Claeys, M., Flagan, R. C., and Seinfeld, J. H.: Organosulfate formation in biogenic secondary organic aerosol, J. Phys. Chem. A, 112, 8345–8378, https://doi.org/10.1021/jp802310p, 2008.

Surratt, J. D., Chan, A. W. H., Eddingsaas, N.C., and Seinfeld, J. H.: Reactive intermediates revealed in secondary organic aerosol formation from isoprene, Proc. Natl. Acad. Sci. U.S.A., 107, 6640–6645, https://doi.org/10.1073/pnas.0911114107, 2010.

Tang, S., Li, F., Tsona, N. T., Lu, C. Y., Wang, X. F., and Du, L.: Aqueous-phase photooxidation of vanillic acid: A potential source of Humic-Like Substances (HULIS), ACS Earth Space Chem., 4, 862–872, https://doi.org/10.1021/acsearthspacechem.0c00070, 2020.

Thomas, A. E., Glicker, H. S., Guenther, A. B., Seco, R., Vega Bustillos, O., Tota, J., Souza, R. A. F., and Smith, J. N.: Seasonal investigation of ultrafine-particle organic composition in an eastern Amazonian rainforest, Atmos. Chem. Phys., 25, 959–977, https://doi.org/10.5194/acp-25-959-2025, 2025.

Tolocka, M. P., and Turpin, B.: Contribution of organosulfur compounds to organic aerosol mass, Environ. Sci. Technol., 46, 7978–7983, https://doi.org/10.1021/es300651v, 2012.

Tsona T. N., Lv, X., Tasheh, S. N., Ghogomu, J. N., and Du, L.: Atmospheric fate of organosulfates through gas-phase and aqueous-phase reactions with hydroxyl radicals: implications for inorganic sulfate formation, Atmos. Chem. Phys., 25, 8575–8590, https://doi.org/10.5194/acp-25-8575-2025, 2025.

Wang, L., Wu, R., and Xu, C.: Atmospheric oxidation mechanism of benzene. fates of alkoxy radical intermediates and revised mechanism, J. Phys. Chem. A, 117, 14163–14168, https://doi.org/10.1021/jp4101762, 2013.

Wang, S., Zhou, S., Tao, Y., Tsui, W. G., Ye, J., Yu, J.Z., Murphy, J. G., McNeill, V. F., Abbat, J. P. D., and Chan, A. W. H.: Organic peroxides and sulfur dioxide in aerosol: source of particulate sulfate, Environ. Sci. Technol., 53, 10695–10704, https://doi.org/10.1021/acs.est.9b02591, 2019.

Wang, Y., Hu, M., Guo, S., Wang, Y., Zheng, J., Yang, Y., Zhu, W., Tang, R., Li, X., Liu, Y., Le Breton, M., Du, Z., Shang, D., Wu, Y., Wu, Z., Song, Y., Lou, S., Hallquist, M., and Yu, J.: The secondary formation of organosulfates under interactions between biogenic emissions and anthropogenic pollutants in summer in Beijing, Atmos. Chem. Phys., 18, 10693–10713, https://doi.org/10.5194/acp-18-10693-2018, 2018.

Wang, Y., Ma, Y., Kuang, B., Lin, P., Liang, Y., Huang, C., and Yu, J. Z.: Abundance of organosulfates derived from biogenic volatile organic compounds: Seasonal and spatial contrasts at four sites in China, Sci. Total Environ., 806, 151275, https://doi.org/10.1016/j.scitotenv.2021.151275, 2022.

Wang, Y., Zhao, Y., Wang, Y., Yu, J.-Z., Shao, J., Liu, P., Zhu, W., Cheng, Z., Li, Z., Yan, N., and Xiao, H.: Organosulfates in atmospheric aerosols in Shanghai, China: seasonal and interannual variability, origin, and formation mechanisms, Atmos. Chem. Phys., 21, 2959–2980, https://doi.org/10.5194/acp-21-2959-2021, 2021.

Xu, R., Ge, Y., Kwong, K. C., Poon, H. Y., Wilson, K. R., Yu, J. Z., and Chan, M. N.: Inorganic sulfur species formed upon

heterogeneous •OH oxidation of organosulfates: A case study of methyl sulfate, ACS Earth Space Chem., 4, 2041–2049, https://doi.org/10.1021/acsearthspacechem.0c00209, 2020.

Xu, R., Ng, S. I. M., Chow, W. S., Wong, Y. K., Wang, Y., Lai, D., Yao, Z., So, P.-K., Yu, J. Z., and Chan, M. N.: Chemical transformation of α-pinene-derived organosulfate via heterogeneous OH oxidation: implications for sources and environmental fates of atmospheric organosulfates, Atmos. Chem. Phys., 22, 5685–5700, https://doi.org/10.5194/acp-22-5685-2022, 2022.

Xu, R., Chen, Y., Ng, S. I. M., Zhang, Z, Gold, A., Turpin, B. J., Ault, A. P., Surratt, J.D., and Chan, M. N.: Formation of inorganic sulfate and volatile nonsulfated products from heterogeneous hydroxyl radical oxidation of 2-methyltetrol sulfate aerosols: Mechanisms and atmospheric implications, Environ. Sci. Technol. Lett., 11, 968–974, https://doi.org/10.1021/acs.estlett.4c00451, 2024.

Yan, J.; Zhang,Y.; Chen,Y.; Armstrong, N.C.; Buchenau, N. A.; Lei, Z.; Xiao,Y.; Zhang, Z.; Lambe, A. T.; Chan,M.N. Kinetics and products of heterogeneous hydroxyl radical oxidation of isoprene epoxydiol-derived secondary organic aerosol. ACS Earth Space Chem. 2023, 7, 1916.

Yang, T., Xu, Y., Ye, Q., Ma, Y.-J., Wang, Y.-C., Yu, J.-Z., Duan, Y.-S., Li, C.-X., Xiao, H.-W., Li, Z.-Y., Zhao, Y., and Xiao, H.-Y.: Spatial and diurnal variations of aerosol organosulfates in summertime Shanghai, China: potential influence of photochemical processes and anthropogenic sulfate pollution, Atmos. Chem. Phys., 23, 13433–13450, https://doi.org/10.5194/acp-23-13433-2023, 2023.

Yao, M., Zhao, Y., Hu, M., Huang, D., Wang, Y., Yu, J. Z., and Yan, N.: Multiphase reactions between secondary organic aerosol and sulfur dioxide: kinetics and contributions to sulfate formation and aerosol aging, Environ. Sci. Technol. Lett., 6, 768–774, https://doi.org/10.1021/acs.estlett.9b00657, 2019.

Yao, M., Zhao, Y., Chang, C. X., Wang, S., Li, Z., Li, C., Chan, A, W, H., and Xiao, H.: Multiphase reactions between organic peroxides and sulfur dioxide in internally mixed inorganic and organic particles: key roles of particle phase separation and acidity, Environ. Sci. Technol., 57, 15558–15570, https://doi.org/10.1021/acs.est.3c04975, 2023.

~~Yu, L., Smith, J., Laskin, A., Anastasio, C., Laskin, J., and Zhang, Q.: Chemical characterization of SOA formed from aqueous-phase reactions of phenols with the triplet excited state of carbonyl and hydroxyl radical, Atmos. Chem. Phys., 14, 13801–13816, https://doi.org/10.5194/acp-14-13801-2014, 2014.~~

Zhang, H., Worton, D. R., Lewandowski, M., Ortega, J., Rubitschun, C. L., Park, J-H., Kristensen, K., Campuzano-Jost, P., Day, D. A., Jimenez, J. L., Jaoui, M., Offenberg, J. H., Kleindienst, T. E., Gilman, T. E., Gilman, J., Kuster, W. C., Gouw, J., Park, C., Schade, G. W., Frossard, A. A., Russell, L., Kaser, L., Jud, W., Hansel, A., Cappellin. L., Karl, T., Glasius, M., Guenther, A., Goldstein, A. H., Seinfeld, J. H., Gold, A., Kamens, R. M., and Surratt, J. D.: Organosulfates as tracers for secondary organic aerosol (SOA) formation from 2-Methyl-3-Buten-2-ol (MBO) in the atmosphere, Environ. Sci. Technol., 46, 9437–9446, https://doi.org/10.1021/es301648z, 2012.